

Triaxiality and non-thermal gas pressure in Abell 1689

Andrea Morandi^{1*}, Marceau Limousin^{2,3}, Yoel Rephaeli^{1,4}, Keiichi Umetsu⁵,
Rennan Barkana¹, Tom Broadhurst^{1,6,7}, Håkon Dahle⁸

¹ *Raymond and Beverly Sackler School of Physics and Astronomy, Tel Aviv University, Tel Aviv, 69978, Israel*

² *Laboratoire d'Astrophysique de Marseille, Université de Provence, CNRS, 38 rue Frédéric Joliot-Curie, F-13388 Marseille Cedex 13, France*

³ *Dark Cosmology Centre, Niels Bohr Institute, University of Copenhagen, Juliane Maries Vej 30, DK-2100 Copenhagen, Denmark*

⁴ *Center for Astrophysics and Space Sciences, University of California, San Diego, La Jolla, CA 92093, USA*

⁵ *Institute of Astronomy and Astrophysics, Academia Sinica, P. O. Box 23-141, Taipei 10617, Taiwan*

⁶ *Department of Theoretical Physics, University of Basque Country UPV/EHU, Leioa, Spain*

⁷ *IKERBASQUE, Basque Foundation for Science, 48011, Bilbao, Spain*

⁸ *Institute of Theoretical Astrophysics, University of Oslo, P.O. Box 1029, Blindern, N-0315 Oslo, Norway*

ABSTRACT

Clusters of galaxies are uniquely important cosmological probes of the evolution of the large scale structure, whose diagnostic power depends quite significantly on the ability to reliably determine their masses. Clusters are typically modeled as spherical systems whose intracluster gas is in strict hydrostatic equilibrium (i.e., the equilibrium gas pressure is provided entirely by thermal pressure), with the gravitational field dominated by dark matter, assumptions that are only rough approximations. In fact, numerical simulations indicate that galaxy clusters are typically triaxial, rather than spherical, and that turbulent gas motions (induced during hierarchical merger events) provide an appreciable pressure component. Extending our previous work, we present results of a joint analysis of X-ray, weak and strong lensing measurements of Abell 1689. The quality of the data allows us to determine both the triaxial shape of the cluster and the level of non-thermal pressure that is required if the intracluster gas is in hydrostatic equilibrium. We find that the dark matter axis ratios are 1.24 ± 0.13 and 2.02 ± 0.01 on the plane of the sky and along the line of sight, respectively, and that about 20% of the pressure is non-thermal. Our treatment demonstrates that the dynamical properties of clusters can be determined in a (mostly) bias-free way, enhancing the use of clusters as more precise cosmological probes.

Key words: cosmology: observations – galaxies: clusters: general – galaxies: clusters: individual (Abell 1689) – gravitational lensing: strong – gravitational lensing: weak – X-rays: galaxies: clusters

1 INTRODUCTION

Clusters of galaxies are the largest bound systems, formed at relatively late times. As such, their mass function sensitively depends on the evolution of the large scale structure (LSS) and on the basic cosmological parameters. Given this great potential, the use of clusters as a cosmological probe hinges on our ability to accurately determine their masses.

Mass determinations based on X-ray observations customarily assume spherical symmetry and strict hydrostatic equilibrium (HE), i.e., that intracluster (IC) gas pressure is provided entirely by thermal motions, $P_{\text{tot}} = P_{\text{th}}$. Under

these assumptions X-ray measurements can be successfully used to constrain the mass profile (Sarazin 1988).

In addition to this X-ray based method, optical observations of giant arcs and multiple images produced by strong gravitational lensing (SL) in the central parts of clusters and slight distortions of background sources in the weak lensing (WL) regime allow us to determine projected cluster masses without invoking the assumption of hydrostatic equilibrium (Miralda-Escude & Babul 1995), but an a priori assumption about the spherical symmetry is still often used to deduce the three-dimensional mass profiles.

However, N-body simulations indicate that dark matter (DM) halos are triaxial with intermediate-major and minor-intermediate axis ratios typically of the order of ~ 0.8 (Wang & White 2009), and hydrodynamical nu-

* E-mail: andrea@wise.tau.ac.il

merical simulations suggest that even after equilibrium is established a significant fraction of the pressure support against gravity comes from subsonic non-thermal gas motions (Lau et al. 2009; Zhang et al. 2010; Richard et al. 2010; Meneghetti et al. 2010), raising doubts on the viability of cluster sphericity and purely thermal gas pressure.

Moreover, since lensing is sensitive to the integrated mass contrast along the line of sight, both departures from the spherical assumption (Morandi et al. 2010) and the inclusion of non-thermal pressure support (Molnar et al. 2010) can explain the long-standing discrepancy between cluster masses determined from X-ray and gravitational lensing observations, the latter often being significantly higher than the former.

The main goal of our work is to resolve these discrepancies between X-ray and gravitational lensing mass for the cluster Abell 1689 (Andersson & Madejski 2004; Lemze et al. 2008; Riemer-Sørensen et al. 2009; Peng et al. 2009; Morandi et al. 2011). We tackle this by developing a novel method in order to infer both the desired triaxial shape and physical properties of clusters and the non-thermal pressure via a joint X-ray, weak and strong lensing analysis.

We extend the findings of our previous work on Abell 1689 (Morandi et al. 2011), where we combined X-ray and strong lensing data; in that work we accounted for the three-dimensional geometry, which allowed us to resolve the discrepancy between the mass determined from X-ray and strong gravitational lensing observations in the inner region ($R \lesssim 400$ kpc), assuming strict HE. In the present paper we jointly analyze also weak lensing data that map the projected mass profile out to ~ 3 Mpc. With this additional data we are also able to determine the non-thermal pressure of the IC gas.

Hereafter we assume the flat Λ CDM model, with matter density parameter $\Omega_m = 0.3$, cosmological constant density parameter $\Omega_\Lambda = 0.7$, and Hubble constant $H_0 = 70 \text{ km s}^{-1} \text{ Mpc}^{-1}$. Unless otherwise stated, quoted errors are at the 68.3% confidence level.

2 DATASETS AND ANALYSIS

A full description of the X-ray and SL analysis can be found in Morandi et al. (2011); for details on the WL analysis we refer to Umetsu et al. (2009). Here we only briefly summarize the most relevant or novel aspects of our data reduction and analysis of Abell 1689.

2.1 X-ray analysis

We analyzed two sets of *Chandra* observations (ID numbers 6930 and 7289) from the NASA HEASARC archive with a total exposure time of approximately 150 ks. With respect to Morandi et al. (2011), we repeated the X-ray data reduction and analysis by implementing the most recent *Chandra* calibrations: we used the CIAO software (version 4.3) and the gain file provided within CALDB (version 4.4.3). We measured the gas density profile in a non-parametric way from the surface brightness recovered by a spatial analysis, and we inferred the projected temperature profile by analyzing the spectral data.

The X-ray images were extracted from the two event

files in the energy range 0.5–5.0 keV, then corrected by the exposure map to remove the vignetting effects, followed by the masking out of point sources. We constructed a set of $n = 57$ elliptical annuli of minor radius r_m around the centroid of the surface brightness with eccentricity $e_{b'}(r)$ fixed to that predicted from the eccentricity $e_{b'}(r)^1$ of the DM halo on the plane of the sky as determined from the SL data (see Section 2.4 and Morandi et al. (2010)). We then deduced the electron density $n_e = n_e(r; \epsilon_{c'})$ by deprojecting the surface brightness profile, obtaining $n = 57$ radial measurements in ellipsoidal shells. Note the dependence of $n_e(r; \epsilon_{c'})$ on the eccentricity $\epsilon_{c'}$ of the IC gas along the line of sight, still to be determined (for further details see below and also Appendix A of Morandi et al. 2010).

The spectral analysis was performed by extracting the source spectra from n^* ($n^* = 9$) elliptical annuli of minor radius r_m^* around the centroid of the surface brightness and with eccentricity as predicted from that of the DM halo (as above). For each of the n^* annuli the spectrum was analyzed by simultaneously fitting absorbed MEKAL models to the two observations, in the energy range 0.6–7 keV (0.9–7 keV for the outermost annulus only); we fixed the redshift to $z = 0.183$ and the photoelectric absorption to the Galactic value. For each of the annuli, we considered three free parameters in the spectral analysis: the normalization of the thermal spectrum $K_i \propto \int n_e^2 dV$, the emission-weighted temperature $T_{\text{proj},i}^*$, and the metallicity Z_i .

2.2 Strong lensing analysis

For the strong lensing analysis we refer to the findings of Limousin et al. (2007), who presented a reconstruction of the mass distribution of the galaxy cluster Abell 1689 using detected strong lensing features from deep ACS observations and extensive ground based spectroscopy. They presented a parametric strong lensing mass reconstruction using 34 multiply imaged systems, and they inferred two large-scale dark matter clumps, one associated with the center of the cluster and the other with a northeastern substructure. We masked out the north-eastern sector of both the 2D projected mass map and the X-ray data, in order to avoid the contribution from this secondary substructure. We masked out also the central 25 kpc, which is affected by the mass distribution of the cD galaxy. From the strong lensing analysis the major clump of the cluster appears to be elongated with a major-minor axial ratio on the plane of the sky of 1.24 ± 0.13 and a position angle of 0.4 ± 1 degrees. We rebinned the two-dimensional projected mass map into elliptical annuli, whose eccentricity, centroid and position angle are the same as those inferred from Limousin et al. (2007). Then we calculated average values of the elliptical projected mass profile $\Sigma(R)$, R being the minor radius of the two-dimensional elliptical annuli. We also calculated the covariance matrix C_{sl} among all the measurements of $\Sigma(R)$ similarly to the WL analysis (see §2.3 for further details).

¹ $e_{b'} = \sqrt{1 - (b'/a')^2}$, $a'(b')$ being the major (minor) axis on the plane of the sky.

2.3 Weak lensing analysis

For the weak lensing analysis we refer to the findings of Umetsu et al. (2009), who derived a projected two-dimensional mass map of Abell 1689 based on an entropy-regularized maximum likelihood combination of lens magnification with distortion of red background galaxies in deep Subaru images. Advantages of that approach are: 1) by combining the distortion and magnification measurements the convergence can be obtained unambiguously with the correct mass normalization, while the convergence derived from distortion data alone suffers from the mass-sheet degeneracy; 2) the method is not restricted to the weak regime but applies to the whole area outside the tangential critical curve, where nonlinearity between the surface mass density and the observables extends out to a radius of a few arcminutes. In the two-dimensional projected mass map in WL we masked out the region corresponding to the secondary substructure seen in the SL regime (§2.2), and then rebinned the data into elliptical annuli, whose eccentricity, centroid, and position angle are the same as that from SL.

In order to calculate average values of the elliptically-symmetric projected mass profile $\Sigma(R)$, where R is the minor radius of the two-dimensional elliptical annuli, we compute $\Sigma = \Sigma(R)$ from a weighted radial projection of the two-dimensional surface mass density Σ . Following Hobson & Maisinger (2002), we can formally express a linear relation between Σ and Σ :

$$\Sigma = \mathcal{M}(\mathbf{r}) \Sigma + \mathcal{N}, \quad (1)$$

where \mathcal{N} is the noise vector (at the i 'th pixel) with covariance matrix \mathcal{C} , and $\mathcal{M} = \mathcal{M}(W)$ is the 1D-to-2D mapping matrix. \mathcal{M} is defined as an $N_{\text{pix}} \times N_{\text{ann}}$ matrix, with N_{pix} the total number of pixels, N_{ann} the total number of elliptical annuli, and elements $\mathcal{M}_i^m = W_{im}$, where W_{im} ($0 \leq W_{im} \leq 1$) is the fraction of the area of the i 'th pixel lying within the m 'th elliptical bin. An optimal solution for this problem is given by:

$$\Sigma = (\mathcal{M}^t \mathcal{C}^{-1} \mathcal{M})^{-1} \mathcal{M}^t \mathcal{C}^{-1} \Sigma. \quad (2)$$

The binned surface mass data Σ have covariance matrix \mathcal{C}_{wl} :

$$\mathcal{C}_{\text{wl}} = (\mathcal{M}^t \mathcal{C}^{-1} \mathcal{M})^{-1}. \quad (3)$$

We use Monte Carlo integration to calculate W_{im} , while we refer Σ to the area-weighted minor radius R_m of the m 'th elliptical bin (Umetsu & Broadhurst 2008).

Note that unlike Umetsu & Broadhurst (2008), who used 2D data in order to retrieve best-fit model parameters, in the present paper we used rebinned surface mass profiles. While we verified that this does not change significantly the desired best-fit model parameter (§2.4), fitting rebinned data has the advantage of requiring significant less computational time and it is usually a better approach when it comes to deal with real data, such as WL, possibly affected by systematics. Indeed rebinning involves a smearing of the data and also of their errors (statistical + systematics) on a larger area: provided that the systematics can be regarded as symmetric errors on a large enough area, this is usually a more robust approach than relying on 2D data.

2.4 Joint X-ray+Lensing analysis

Here we briefly summarize the major findings of Morandi et al. (2010) for the joint X-ray+Lensing analysis in order to infer triaxial physical properties; additional details can be found in Morandi et al. (2007, 2010). We also outline the improvements implemented in the present work, i.e., the inclusion of WL data and the measurement of the non-thermal component of the IC gas.

The lensing and the X-ray emission both depend on the properties of the DM gravitational potential well, the former being a direct probe of the two-dimensional mass profile and the latter an indirect proxy of the three-dimensional mass profile through the hydrostatic equilibrium equation applied to the gas temperature and density. In order to infer the model parameters of both the IC gas and of the underlying DM density profile, we perform a joint analysis of SL, WL and X-ray data. We briefly outline the methodology for inferring physical properties in triaxial galaxy clusters: (1) We start with a generalized Navarro, Frenk and White (gNFW) triaxial model of the DM as described in Jing & Suto (2002), which represents the total underlying mass distribution and depends on a few parameters to be determined, namely the concentration parameter c , the scale radius r_s , the inner slope of the DM α and the two axis ratios; (2) following Lee & Suto (2003, 2004), we recover the gravitational potential and surface mass profile Σ of a dark halo with such a triaxial density profile; (3) we solve the generalized hydrostatic equilibrium equation, i.e., including the non-thermal pressure (Equation (4) below), in order to infer the theoretical three-dimensional temperature profile T_{gas} in a non-parametric way, given IC gas with a density profile as deprojected from the X-ray data (see §2.1) and sitting in the gravitational potential well previously calculated; finally, (4) the joint comparison of T_{gas} with the observed temperature and of Σ with the observed surface mass density gives us the parameters of the triaxial DM density model and the non-thermal component of the gas, and therefore all the desired physical properties of the IC gas and the DM triaxial ellipsoids.

In particular, for the X-ray analysis we rely on a generalization of the hydrostatic equilibrium equation (Lau et al. 2009; Molnar et al. 2010), which accounts for the non-thermal pressure P_{nt} and reads:

$$\nabla P_{\text{tot}} = -\rho_{\text{gas}} \nabla \phi, \quad (4)$$

where ρ_{gas} is the gas mass density, ϕ is the gravitational potential, and $P_{\text{tot}} = P_{\text{th}} + P_{\text{nt}}$.

In this first implementation of our new approach, and given the limited ability to carry out a more detailed spatial analysis, we model P_{nt} by assuming that the non-thermal pressure of the gas is a constant fraction ξ of the total pressure P_{tot} , i.e.,

$$P_{\text{nt}} = \xi P_{\text{tot}}. \quad (5)$$

From Equations (4) and (5) we point out that neglecting P_{nt} (i.e., setting $P_{\text{tot}} = P_{\text{th}}$) systematically biases low the determination of cluster masses, roughly by a factor of ξ . Note that X-ray data probe only the thermal component of the gas $P_{\text{th}} = n_e k T_{\text{gas}}$.

The work of Lee & Suto (2003) showed that the IC gas and DM halos are well approximated by a sequence of con-

centric triaxial distributions with different eccentricity ratio. We define $e_{b'}$ ($\epsilon_{b'}$) and $e_{c'}$ ($\epsilon_{c'}$) as the eccentricity of DM (IC gas) on the plane of the sky and along the line of sight, respectively. The iso-potential surfaces of the triaxial dark halo coincide also with the iso-density (pressure, temperature) surfaces of the intracluster gas. This is simply a direct consequence of the *X-ray shape theorem* (Buote & Canizares 1994); the hydrostatic equilibrium equation (4) yields

$$\nabla P \times \nabla \phi = \nabla \rho \times \nabla \phi = 0. \quad (6)$$

Note that $\epsilon_{b'} = \epsilon_{b'}(e_{b'}, u, \alpha)$ and $\epsilon_{c'} = \epsilon_{c'}(e_{c'}, u, \alpha)$, with $\mathbf{u} \equiv \mathbf{r}/r_s$, unlike the constant $e_{b'}$, $e_{c'}$ for the adopted DM halo profile. In the whole range of u , $\epsilon_{b'}/e_{b'}$ ($\epsilon_{c'}/e_{c'}$) is less than unity (~ 0.7 at the center), i.e., the intracluster gas is altogether more spherical than the underlying DM halo.

We construct the likelihood performing a joint analysis for lensing and X-ray data, in order to constrain the properties of the model parameters \mathbf{q}

$$\mathbf{q} = (c, r_s, \alpha, e_{c'}, \xi) \quad (7)$$

representing the concentration parameter, scale radius, inner slope of the DM, eccentricity of the DM along the line of sight and fractional non-thermal pressure of the gas, respectively.

Therefore, the system of equation we simultaneously rely on in our joint X-ray+Lensing analysis is:

$$T_{\text{gas}} = T_{\text{gas}}(c, r_s, \alpha, e_{c'}, \xi) \quad (8a)$$

$$\Sigma = \Sigma(c, r_s, \alpha, e_{c'}) \quad (8b)$$

where the three-dimensional model temperature T_{gas} is recovered by solving equation (4) and constrained by the observed temperature profile, and the model surface mass profile Σ is recovered by projection of the triaxial gNFW DM model and constrained by weak/strong lensing measurements.

The method works by constructing a joint X-ray+Lensing likelihood:

$$\mathcal{L} = \mathcal{L}_X \cdot \mathcal{L}_{\text{lens}} = \mathcal{L}_X \cdot \mathcal{L}_{\text{SL}} \cdot \mathcal{L}_{\text{WL}}, \quad (9)$$

\mathcal{L}_X and $\mathcal{L}_{\text{lens}}$ being the likelihoods coming from the X-ray and lensing (WL+SL) data, respectively. Now, $\mathcal{L}_X \propto \exp(-\chi_X^2/2)$, where

$$\chi_X^2 = \sum_{i=1}^{n^*} \frac{(T_{\text{proj},i} - T_{\text{proj},i}^*)^2}{\sigma_{T_{\text{proj},i}}^2} \quad (10)$$

$T_{\text{proj},i}^*$ being the observed projected temperature profile in the i 'th ring and $T_{\text{proj},i}(\mathbf{q})$ the convenient projection (following Mazzotta et al. 2004) of the theoretical three-dimensional temperature $T_{\text{gas}}(\mathbf{q})$; the latter is the result of solving the hydrostatic equilibrium equation, with the gas density $n_e(r; \epsilon_{c'})$ inferred from the X-ray surface brightness, and assuming a gNFW parametrization for the DM $\rho_{\text{DM}} = \rho_{\text{DM}}(\mathbf{r}; c, r_s, \alpha, e_{c'})$. The lensing contribution is

$$\mathcal{L}_{\text{lens}} = \frac{\exp\left\{-\frac{1}{2}[\Sigma - \Sigma^*]^t \mathbf{C}^{-1}[\Sigma - \Sigma^*]\right\}}{(2\pi)^{m^*/2} |\mathbf{C}|^{1/2}}, \quad (11)$$

where \mathbf{C} is the covariance matrix of the projected mass profile from strong (\mathbf{C}_{sl}) and weak (\mathbf{C}_{wl}) lensing data, $|\mathbf{C}|$ indicates the determinant of \mathbf{C} , $\Sigma^* = (\Sigma_1^*, \Sigma_2^*, \dots, \Sigma_{m^*}^*)$ are the observed measurements of the projected mass profile in

the m^* elliptical annuli, and $\Sigma(c, r_s, \alpha, e_{c'})$ is the theoretical projected mass profile within our triaxial DM model.

For the covariance matrix of the strong lensing measurements, we also account for systematic errors by replacing the observed covariance matrix with the following expression:

$$\mathbf{C}_{\text{sl}} \longrightarrow \mathbf{C}_{\text{sl}} + \sigma_{\text{sys}}^2 \mathcal{I} \quad (12)$$

where \mathcal{I} is the identity matrix. Since we are using the surface mass density as output from the parametric SL analysis of Limousin et al. (2007), we introduce the parameter σ_{sys} to allow some extra freedom due to possible systematic bias resulting from their analysis. In order to calculate σ_{sys} we assumed that systematic errors can be described as Gaussian errors via a diagonal matrix $\sigma_{\text{sys}}^2 \mathcal{I}$ with the same value in each of the diagonal elements. We checked that this simplified assumption does not significantly affect the average value of the physical parameters, while it slightly increases (12%-20%) their errors with respect to the case where we neglect σ_{sys} .

We evaluated the probability distribution function of model parameters $\mathcal{L} = \mathcal{L}(\mathbf{q}, \sigma_{\text{sys}})$ via the Markov Chain Monte Carlo (MCMC) algorithm. Thus we can determine our best-fit model parameters and their errors, and derive various properties of the cluster.

3 RESULTS AND DISCUSSION

In the previous section we showed how we can determine the physical parameters of the cluster by fitting the available data based on the hydrostatic equilibrium equation and on a DM model that is based on robust results of hydrodynamical cluster simulations. In this section we present our results and discuss their main implications. We particularly focus on the implications of our analysis for the viability of the CDM scenario, the discrepancy between X-ray and lensing masses in Abell 1689, and the presence of non-thermal pressure.

3.1 Best-fit parameters

In Figure 1 we present the results of our joint analysis for Abell 1689. Both the X-ray and lensing data are reasonably fitted by our model, with a total $\chi_{\text{tot}}^2 = \chi_X^2 + \chi_{\text{sl}}^2 + \chi_{\text{wl}}^2 = 33.8$ (with 20 degrees of freedom). The separate contributions are $\chi^2 = 12.4, 6.3, 15.1$ for X-ray, SL and WL data, respectively, where $\chi_{\text{lens}}^2 \propto -2 \log(\mathcal{L}_{\text{lens}})$.

Note that in Figure 1 the WL model predictions are slightly in disagreement with the data, overpredicting the surface mass profile in the range 500-2000 kpc at around the 1- σ significance level, while the X-ray and SL data are rather well fitted. We checked that the inclusion of WL data does not significantly change the values of the desired physical parameters. Also, we verified that the joint fit is preferentially more strongly constrained by the X-ray and SL data with the present datasets, WL measurements being of poorer quality. Excluding WL data slightly increases (5%-15%) the errors on the final parameters with respect to the case where we include them, with the exception of P_{nt} , where the error would increase of $\sim 60\%$. With this respect, while for the present datasets WL data are less relevant in constraining the model parameters with respect to X-ray and SL data, whose quality is exceptionally good, we observe that this might not

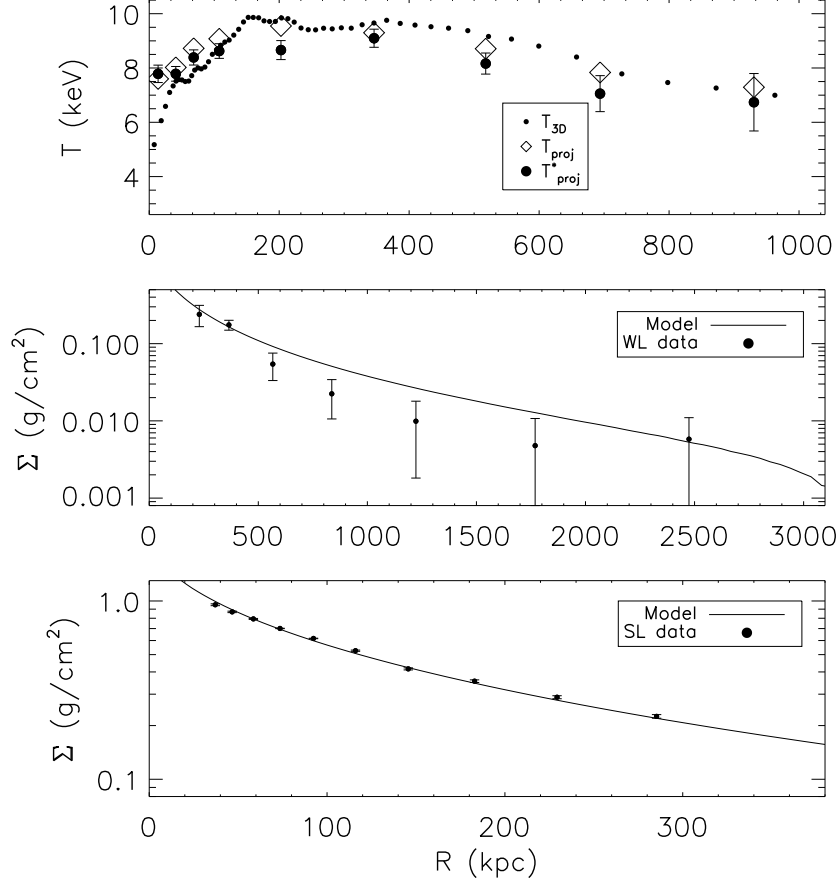


Figure 1. Joint X-ray and lensing analysis for Abell 1689. In the upper panel we display the two quantities that enter in the X-ray analysis (Equation (10)): the observed projected temperature $T_{\text{proj},i}^*$ (big points with error bars) and the theoretical projected temperature $T_{\text{proj},i}(\mathbf{q})$ (diamonds). We also show the theoretical three-dimensional temperature $T_j(\mathbf{q})$ (points), which generates $T_{\text{proj},i}(\mathbf{q})$ through convenient projection techniques. In the middle and lower panel we display the two quantities which enter in the WL and SL analysis, respectively (Equation (11)): the observed surface mass profile Σ_i^* (points with error bars) and the theoretical one $\Sigma(\mathbf{q})$ (solid line). The distance of the points for both $T_j(\mathbf{q})$ and Σ_i^* is representative of the true spatial resolution of X-ray and lensing data, respectively.

apply for other galaxy clusters and other datasets, where the inclusion of WL data could be important in removing the degeneracy among the same parameters.

To further probe the disagreement between WL and SL data, we jointly fitted them (without the X-ray data) with a spherical NFW ($\alpha = 1$) model first (following Umetsu & Broadhurst (2008)), and then with the more general triaxial gNFW. We found a marginal disagreement between SL and WL data for both models. A similar slight disagreement can also be seen in Figure 13 of Umetsu & Broadhurst (2008).

In order to make a comparison with Morandi et al. (2011), we also compared the χ^2 by neglecting WL data and without P_{nt} : we find $\chi^2 = 25.3$ (14 degrees of freedom), while in Morandi et al. (2011) we found that the $\chi^2 \sim 7.4$ (11 degrees of freedom). Note that the difference in the value of the χ^2 reflects a different treatment of the SL data in the present paper (§2.2 and §2.3) in comparison to our previous work. Among these difference, the major improvement is based on the determination of covariance C_{sl} among the pixels of the 2D map distribution, in order to infer the co-

variance C_{sl} among the rebinned measurements (Equation 3), and on an improved rebinning schema (Equation 2). We also point out that this difference in the value of the χ^2 translates to slightly different errors in the parameter values, with negligible impact on their expectation values. For example, we find that the axis ratio along the line of sight $\eta_{\text{DM},c'} = 2.39 \pm 0.02$ (by neglecting WL data and without P_{nt}), whereas the value deduced in Morandi et al. (2011) was $\eta_{\text{DM},c'} = 2.37 \pm 0.11$.

In Table 1 we present the best-fit model parameters for our analysis of Abell 1689. Errors in the individual parameters ($\mathbf{q}, \sigma_{\text{sys}}$) have been evaluated by considering the average value and the mean absolute deviation of the marginal probability distribution of each parameter. Note that we list the axis ratio along the line of sight $\eta_{\text{DM},c'}$ rather than the eccentricity. Our work shows that Abell 1689 is a triaxial galaxy cluster with DM halo axis ratios $\eta_{\text{DM},b'} = 1.24 \pm 0.13$ and $\eta_{\text{DM},c'} = 2.02 \pm 0.01$, where $\eta_{\text{DM},b'}$ is the axis ratio on the plane of the sky inferred from SL measurements, and $\eta_{\text{DM},c'}$ is the axis ratio along the line of sight inferred through our joint analysis. Note that these elongations are statistically

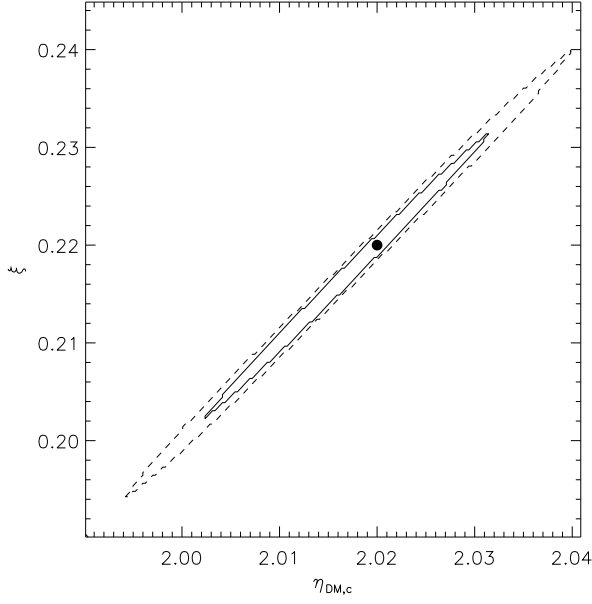


Figure 2. Joint probability distribution of $\eta_{\text{DM},c'}$ and ξ . The solid(dashed) line represents the 1(2)- σ error region, while the big dot represents the best-fit values.

significant, i.e., our results disprove the spherical geometry assumption. The axis ratio of the gas is $\eta_{\text{gas},b'} \sim 1.1 - 1.06$ (on the plane of the sky) and $\eta_{\text{gas},c'} \sim 1.5 - 1.3$ (along the line of sight), moving from the center toward the X-ray boundary.

In Table 1 we also report the value of M_{200} :

$$M_{200} = \frac{800\pi}{3} (a_r/c_r)(b_r/c_r) R_{200}^3 \rho_c, \quad (13)$$

where ρ_c is the critical density of the Universe at the redshift z of the cluster, $c = R_{200}/r_s$, and a_r/c_r and b_r/c_r are the minor-major and intermediate-major axis ratios of the DM halo, respectively.

The second main result from our work is the need for a appreciable non-thermal pressure support, formally at a level of $\sim 20\%$.

In Figure 2 we present the joint probability distribution of $\eta_{\text{DM},c'}$ and ξ . Note the positive correlation between ξ and $\eta_{\text{DM},c'}$, i.e. the X-ray/Lensing mass discrepancy in clusters with prominent strong lensing features can be explained via a combination of both triaxiality and non-thermal support. This expected in light of the following considerations: (1) the observed temperature profile and projected mass profile are both sensitive to triaxiality, specifically $T(R, \eta_{\text{DM}}) \sim \eta_{\text{gas},c'} T(R, \eta_{\text{DM}} = 1)$ and $\Sigma(R) \propto \eta_{\text{DM},c'}$ (Morandi et al. 2010), so that the dependency of $\Sigma(R)$ on triaxiality is stronger than that of $T(R)$ (remembering that generally $\eta_{\text{DM},c'} > \eta_{\text{gas},c'}$); (2) the non-thermal pressure support affects only the X-ray data via Equation 4, i.e., neglecting P_{nt} systematically lowers the determination of cluster masses based on X-ray data roughly by the factor ξ .

3.2 Implications for the viability of the CDM scenario and the X-ray/Lensing mass discrepancy

A precise determination of cluster masses is crucial for the use of clusters as cosmological probes. However, there are discrepancies between cluster masses determined based on gravitational lensing and on X-ray observations, the former being significantly higher than the latter in many clusters with prominent lensing features. Indeed, Oguri & Blandford (2009) showed that SL clusters with the largest Einstein radii constitute a highly biased population with major axes preferentially aligned with the line of sight thus increasing the magnitude of lensing. Given that lensing depends on the integrated mass along the line of sight, either fortuitous alignments with mass concentrations that are not physically related to the galaxy cluster or departures of the DM halo from spherical symmetry can bias upwards the three-dimensional mass with respect to the X-ray mass (Gavazzi 2005); on the other hand, X-ray-only masses hinge on the accuracy of the assumption of strict hydrostatic equilibrium: the presence of bulk motions in the gas can bias low the three-dimensional mass profile between 5 and 20% (Meneghetti et al. 2010).

Oguri et al. (2005) concluded that weak lensing measurements in Abell 1689 are indeed compatible with the CDM-based triaxial halo model if Abell 1689 represents a rare population ($\sim 6\%$ by number) of cluster-scale halos, and Morandi et al. (2011) demonstrated that triaxiality allows us to remove the mass discrepancy between the strong lensing and X-ray estimates in Abell 1689. Molnar et al. (2010) suggested an alternative explanation for the mass discrepancy, due to violations of strict hydrostatic equilibrium in Abell 1689: they found that a contribution of about 40% from non-thermal pressure within the core region of Abell 1689 can explain the mass discrepancy, provided that the spherical geometry assumption holds.

Moreover, recent work investigating the mass distributions of individual galaxy clusters (Abell 1689 and others) based on gravitational lensing and employing standard spherical modeling have found a potential inconsistency compared to the predictions of the CDM scenario relating halo mass to the concentration parameter c . In particular, relatively high values of c ($\sim 8-14$) have been derived from lensing analysis of Abell 1689 (Broadhurst et al. 2005; Limousin et al. 2007). These values are outside the range predicted from simulations of the standard CDM model ($c \sim 4$; Neto et al. 2007).

In the present work we presented a physical model for the cluster Abell 1689 with a triaxial mass distribution including support from non-thermal pressure. This model is consistent with X-ray and SL observations as well as with the predictions of the CDM model. Doing so we have removed the apparent discrepancy between X-ray and lensing mass estimates, and potential inconsistencies discussed in the literature between the predictions of the CDM scenario and the measurements in clusters with prominent strong lensing features. One of the main results of our work is the measurement of a central slope of the DM profile 0.95 ± 0.05 in agreement with the theoretical expectation of the CDM scenario (Navarro et al. 1997; Merritt et al. 2006), and a value of the concentration parameter 5.71 ± 0.47 , in agreement

Table 1. Best-fit model parameters of A1689. The columns 1–6 refer to the best fit parameters c , r_s , α , $\eta_{DM,c'}$, ξ and σ_{sys} , while the last column refers to M_{200} .

c	r_s (kpc)	α	$\eta_{DM,c'}$	ξ	σ_{sys} (g cm $^{-2}$)	M_{200} ($10^{15} M_\odot$)
5.71 ± 0.47	348 ± 28	0.95 ± 0.05	2.02 ± 0.01	0.22 ± 0.01	0.008 ± 0.001	2.59 ± 0.09

with the theoretical expectation from N-body simulations of Neto et al. (2007), where $c \sim 4$ at the redshift and for the virial mass of Abell 1689, with an intrinsic scatter of $\sim 20\%$. In this way we also managed to reproduce the large Einstein radius of Abell 1689 via our triaxial framework (Morandi et al. 2011).

Even with triaxiality, though, Oguri et al. (2005) found that Abell 1689 is relatively rare in its lensing efficiency, as noted above. Furthermore, Broadhurst & Barkana (2008) showed that the observed Einstein radius θ_E of four well-studied massive clusters (including Abell 1689) lies well beyond the predicted distribution of Einstein radii in the standard CDM model, typically by a factor of 2, even after accounting for the actual projected mass distributions in N-body simulations, and for lensing bias. Using a larger sample of 12 X-ray selected clusters, Zitrin et al. (2011) found a smaller discrepancy with CDM predictions, typically by a factor of 1.4.

In a similar fashion, by comparing numerical and observational cluster samples, Meneghetti et al. (2011) show that some real clusters have too large lensing cross sections and Einstein rings compared to expectations in a Λ CDM cosmological model. Horesh et al. (2011) partially confirmed these results, by comparing the lensed arc statistics measured from the Millennium simulation to those of a sample of observed clusters: they found an excellent agreement between the observed and simulated number of arcs in the redshift range $0.3 < z < 0.5$, while at lower redshift some conflict still remains, with real clusters being ~ 3 times more efficient arc producers than their simulated counterparts. This departure might be due to selection biases in the observed subsample at this redshift or to physical effects that arise at low redshift and enhance the lensing efficiency, and not included the simulations, as the effect of baryons on the DM profile in clusters (Barkana & Loeb 2010).

We also compare the major-minor principal axis ratio $\eta_{DM,c'} = 2.02 \pm 0.01$ with that inferred in our previous work ($\eta_{DM,c'} = 2.37 \pm 0.11$; Morandi et al. 2011). The estimated value of the elongation along the line of sight in the present work is somewhat smaller, due to the assumption of strict hydrostatic equilibrium and the lack of the large-scale WL data in our previous work. This lends further support to our emphasis on the role of the effects of both geometry and non-thermal pressure support on the physical parameters and open a new window in recovering the intrinsic shapes and desired physical parameters of galaxy clusters in a bias-free way. The estimated value of $\eta_{DM,c'}$ is also consistent with the results from numerical simulations (Shaw et al. 2006).

3.3 Non-thermal gas pressure

Simulations of galaxy clusters predict that turbulent motions should occur in the IC gas while the matter continues to accrete along filaments. This energy should then cascade from large to small scales and can eventually dissipate into the gas. The attainment of HE does not by itself rule out an appreciable level of turbulence ($\sim 5\text{--}15\%$, Lau et al. 2009; Zhang et al. 2010). Measurements of the non-thermal energy in the IC gas are important in order to estimate the amount of energy injected into clusters from mergers, accretion of material or feedback from active galactic nuclei (AGNs); in the latter case, this probes energy transport from the central nucleus into its surroundings and into the IC gas. Brüggen et al. (2005) found that in clusters with AGN feedback gas motion induced by the inflation of bubbles and their buoyant rise leads to velocities of about $500\text{--}1000 \text{ km s}^{-1}$, which is a significant fraction of the local sound speed. Strong turbulent motions would provide significant non-thermal pressure support; this would bias low the determination of cluster mass profiles measured under the assumption that $P_{tot} = P_{th}$ in Equation (4). The measurement of turbulence is thus important for mass determination as well as understanding AGN feedback. Moreover, Molnar et al. (2010) argued that there is no need for feedback from a central AGN for the strict hydrostatic equilibrium to break down in the central regions of clusters: subsonic random gas motions, a direct consequence of hierarchical structure formation, allow us to explain violations of the strict hydrostatic equilibrium assumption in the central regions; in the outer regions violations could be due to more recent and still ongoing slow accretion, since those regions have not reached equilibrium due to the large sound crossing time.

Observationally, Richard et al. (2010) measured an X-ray/Lensing mass discrepancy of $< M_{sl}/M_x > = 1.3$ at $3\text{--}\sigma$ significance level in a sample of 20 strong lensing clusters. They interpret this as evidence that the assumption of strict hydrostatic equilibrium required by the X-ray mass estimates is not wholly reliable and the merging activity can add non-thermal pressure support to the IC gas through bulk motions. Sanders et al. (2010) placed a direct limit on turbulence based on the non-thermal velocity broadening measured from the emission lines originating in the central 30 kpc of the galaxy cluster Abell 1835. They found that the ratio of turbulent to thermal energy density in the core is less than 13%.

Molnar et al. (2010) analyzed a sample of massive clusters of galaxies drawn from high-resolution cosmological sim-

ulations and found a significant contribution (20%-45%) from non-thermal pressure. They also tested the validity of strict hydrostatic equilibrium in Abell 1689 using gravitational lensing and X-ray observations under the assumption of spherical geometry in order to explain the X-ray/Lensing mass discrepancy: they found a contribution of about 40% from non-thermal pressure within the core region of Abell 1689, suggesting an alternate explanation for the mass discrepancy, as long as the spherical assumption holds.

Our results point to a scenario where the non-thermal component is about 20% of the total energy budget of the IC gas. This level is quite lower than that found from Molnar et al. (2010) under the assumption of spherical geometry, suggesting that accounting for the proper triaxial geometry is quite important in evaluating P_{nt} accurately.

Another relevant consideration here is that in our model we constrained the non-thermal pressure to be a constant factor of the local thermal pressure throughout the cluster. The results of Mahdavi et al. (2008) show that there is a radial trend of the X-ray/WL mass ratio, that is interpreted as caused by non-thermality increasing toward the outer regions, though their findings hinge on the assumed spherical geometry, so they did not disentangle the effect of triaxiality from non-thermal pressure support. In this perspective, we used a linear relation of P_{nt} , by fixing the slope to that found by Mahdavi et al. (2008) and leaving the normalization as a free parameter: the results are not affected appreciably from this, the reason is that the fit is more dominated by the innermost part (< 300 kpc) of the X-ray and SL data. Moreover, in order to gauge the likely model dependence of the inferred non-thermal pressure, we performed a joint analysis by excluding the temperature constraints (Equation 10) and assuming a spherical NFW model for the DM. Doing so also allows us to make a direct comparison with Lemze et al. (2008), who used a similar approach. We found that the ratio between the (de)-projected temperature profile measured from the X-ray spectrum and that obtained by assuming strict hydrostatic equilibrium (Equation 4 with $P_{\text{tot}} = P_{\text{th}}$) is $\sim 0.5 - 0.6$, which is lower than the determination in our triaxial model ($P_{\text{th}}/P_{\text{tot}} \sim 0.8$). Note that Lemze et al. (2008) concluded that a factor of 0.7 explains most of the temperature discrepancy in Abell 1689, whereas we find a somewhat lower value; this stems mostly from the more recent Chandra calibrations adopted in the present work, which led to a lower spectral temperature profile (by $\sim 20\%$). While this test heavily hinges on the model of spherical geometry, it suggests that the small formal error on ξ in our triaxial joint analysis merits some caution.

4 SUMMARY AND CONCLUSIONS

In this paper we have employed a physical cluster model for Abell 1689 with a triaxial mass distribution including support from non-thermal pressure, and proved that it is consistent with the X-ray and SL observations and the predictions of CDM models.

We demonstrated that accounting for the three-dimensional geometry and the non-thermal component of the gas allows us to resolve the long-standing discrepancy between the X-ray and strong lensing mass of Abell 1689 in

the literature, as well as to measure a central slope of the DM and a concentration parameter in agreement with the theoretical expectations of the CDM scenario.

We also measured the contribution of the non-thermal component of the gas ($\sim 20\%$ of the total energy budget of the IC gas). This has important consequences for estimating the amount of energy injected into clusters from mergers, accretion of material or feedback from AGN.

The increasing precision of observations now makes it possible to test the assumptions of spherical symmetry and hydrostatic equilibrium. Since important current cosmological tests are based on the knowledge of the masses, shapes, and profiles of galaxy clusters, it is important to better characterize their physical properties by allowing for realistic triaxial structures as well as non-thermal pressure support. The application of our method to a larger sample of clusters will allow to infer the desired physical parameters of galaxy clusters in a bias-free way, with important implications on the use of galaxy clusters as precise cosmological probes.

ACKNOWLEDGEMENTS

A.M. and R.B. acknowledge support by Israel Science Foundation grant 823/09. M.L. acknowledges the Centre National de la Recherche Scientifique (CNRS) for its support. The Dark Cosmology Centre is funded by the Danish National Research Foundation.

REFERENCES

- Andersson K. E., Madejski G. M., 2004, *ApJ*, 607, 190
- Barkana R., Loeb A., 2010, *MNRAS*, 405, 1969
- Broadhurst T., Benítez N., Coe D., Sharon K., Zekser K., White R., Ford H., Bouwens R., Blakeslee J., Clampin M., Cross N., Franx M., Frye B., Hartig G., Illingworth G., 2005, *ApJ*, 621, 53
- Broadhurst T. J., Barkana R., 2008, *MNRAS*, 390, 1647
- Brüggen M., Hoeft M., Ruszkowski M., 2005, *ApJ*, 628, 153
- Buote D. A., Canizares C. R., 1994, *ApJ*, 427, 86
- Gavazzi R., 2005, *A&A*, 443, 793
- Hobson M. P., Maisinger K., 2002, *MNRAS*, 334, 569
- Horeh A., Maoz D., Hilbert S., Bartelmann M., 2011, *ArXiv e-prints*
- Jing Y. P., Suto Y., 2002, *ApJ*, 574, 538
- Lau E. T., Kravtsov A. V., Nagai D., 2009, *ApJ*, 705, 1129
- Lee J., Suto Y., 2003, *ApJ*, 585, 151
- Lee J., Suto Y., 2004, *ApJ*, 601, 599
- Lemze D., Barkana R., Broadhurst T. J., Rephaeli Y., 2008, *MNRAS*, 386, 1092
- Limousin M., Richard J., Jullo E., Kneib J., Fort B., Soucail G., Elíasdóttir Á., Natarajan P., Ellis R. S., Smail I., Czoske O., Smith G. P., Hudelot P., Bardeau S., Ebeling H., Egami E., Knudsen K. K., 2007, *ApJ*, 668, 643
- Mahdavi A., Hoekstra H., Babul A., Henry J. P., 2008, *MNRAS*, 384, 1567
- Mazzotta P., Rasia E., Moscardini L., Tormen G., 2004, *MNRAS*, 354, 10
- Meneghetti M., Fedeli C., Zitrin A., Bartelmann M., Broadhurst T., Gottloeber S., Moscardini L., Yepes G., 2011, *ArXiv e-prints*

- Meneghetti M., Rasia E., Merten J., Bellagamba F., Ettori S., Mazzotta P., Dolag K., Marri S., 2010, *A&A*, 514, A93+
- Merritt D., Graham A. W., Moore B., Diemand J., Terzić B., 2006, *AJ*, 132, 2685
- Miralda-Escude J., Babul A., 1995, *ApJ*, 449, 18
- Molnar S. M., Chiu I., Umetsu K., Chen P., Hearn N., Broadhurst T., Bryan G., Shang C., 2010, *ApJ*, 724, L1
- Morandi A., Ettori S., Moscardini L., 2007, *MNRAS*, 379, 518
- Morandi A., Pedersen K., Limousin M., 2010, *ApJ*, 713, 491
- Morandi A., Pedersen K., Limousin M., 2011, *ApJ*, 729, 37
- Navarro J. F., Frenk C. S., White S. D. M., 1997, *ApJ*, 490, 493
- Neto A. F., Gao L., Bett P., Cole S., Navarro J. F., Frenk C. S., White S. D. M., Springel V., Jenkins A., 2007, *MNRAS*, 381, 1450
- Oguri M., Blandford R. D., 2009, *MNRAS*, 392, 930
- Oguri M., Takada M., Umetsu K., Broadhurst T., 2005, *ApJ*, 632, 841
- Peng E., Andersson K., Bautz M. W., Garmire G. P., 2009, *ApJ*, 701, 1283
- Richard J., Smith G. P., Kneib J., Ellis R. S., Sanderson A. J. R., Pei L., Targett T. A., Sand D. J., Swinbank A. M., Dannerbauer H., Mazzotta P., Limousin M., Egami E., Jullo E., Hamilton-Morris V., Moran S. M., 2010, *MNRAS*, 404, 325
- Riemer-Sørensen S., Paraficz D., Ferreira D. D. M., Pedersen K., Limousin M., Dahle H., 2009, *ApJ*, 693, 1570
- Sanders J. S., Fabian A. C., Smith R. K., Peterson J. R., 2010, *MNRAS*, 402, L11
- Sarazin C. L., 1988, *Journal of the British Astronomical Association*, 98, 212
- Shaw L. D., Weller J., Ostriker J. P., Bode P., 2006, *ApJ*, 646, 815
- Umetsu K., Birkinshaw M., Liu G., Wu J., Medezinski E., Broadhurst T., Lemze D., Zitrin A., Ho P. T. P., Huang C., Koch P. M., Liao Y., Lin K., Molnar S. M., 2009, *ApJ*, 694, 1643
- Umetsu K., Broadhurst T., 2008, *ApJ*, 684, 177
- Wang J., White S. D. M., 2009, *MNRAS*, 396, 709
- Zhang Y., Okabe N., Finoguenov A., Smith G. P., Piffaretti R., Valdarnini R., Babul A., Evrard A. E., Mazzotta P., Sanderson A. J. R., Marrone D. P., 2010, *ApJ*, 711, 1033
- Zitrin A., Broadhurst T., Barkana R., Rephaeli Y., Benítez N., 2011, *MNRAS*, 410, 1939